JACS
JOURNAL OF THE AMERICAN CHEMICAL SOCIETY
pubs.acs.org/JACS
Article

Unraveling the Intrinsic Interfacial Chemistry of Fluoroethylene Carbonate on Lithium Metal Anodes via a Solvent-Free Model System

Nanbiao Pei, Yuan Tian, Xueying Yang, Qijie Gao, Yaqi Zhang, Zhibin Lin, Yu Qiao, Peng Zhang,* and Jinbao Zhao*

Cite This: https://doi.org/10.1021/jacs.6c16437
Read Online

ACCESS | Metrics & More | Article Recommendations | Supporting Information

ABSTRACT: Fluoroethylene carbonate (FEC) is a widely used film-forming additive for stabilizing lithium metal anodes (LMAs), yet its intrinsic interfacial chemistry remains elusive because its reactions are coupled with those of solvents and Li salts in conventional electrolytes. Herein, a solvent-free, dry-processed poly(ethylene oxide)-based solid polymer electrolyte (PEO@Dry) is developed as a platform to isolate the interfacial reactions of FEC without interference from traditional liquid organic solvents. PEO@Dry retains the intrinsic interfacial reactivity of PEO and LiTFSI while eliminating solvent-derived interference. FEC is found to undergo a spontaneous chemical reaction with Li metal before electrochemical reduction, producing a dense LiF-rich solid electrolyte interphase (SEI) that is subsequently reinforced by organic species derived from the electrochemical reactions. The resulting SEI exhibits a well-defined composition and robust structure, leading to an enhanced interfacial stability and electrochemical performance. Comparative research with a DME-based liquid electrolyte reveals that FEC (DME@FEC) follows distinct reaction pathways depending on its solvation state. In the solvent-free PEO@Dry system, free FEC undergoes sequential chemical and electrochemical reduction to form an inorganic-rich SEI, whereas in the liquid electrolyte, FEC participates in Li^+ solvation and competes with other electrolyte components, yielding a more complex SEI. This work clarifies the interfacial mechanism of FEC and establishes a general solvent-free platform for mechanistic studies of electrolyte additives on LMAs.

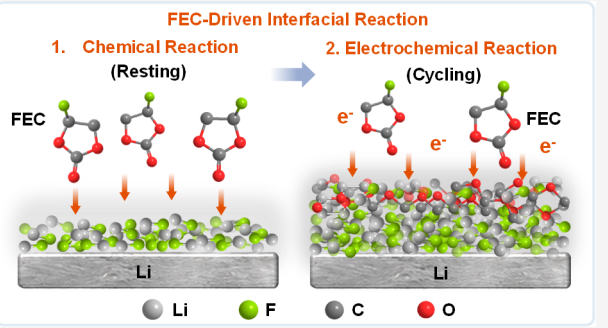

INTRODUCTION

Lithium-ion batteries (LIBs) have been widely applied due to their long lifespan and high energy density,[1−6] but the rising energy density demand for batteries has attracted more attention to lithium metal batteries (LMBs). However, LMBs are associated with problems such as low Coulombic efficiency, short cycle lifespan, and potential safety hazards.[7−10] First, Li metal with the lowest electrode potential (−3.04 V) will cause a violent interfacial side reaction on the LMA, which is accompanied by the continuous consumption of active Li metal and leading to low Coulombic efficiency.[11−14] Meanwhile, a high nucleation overpotential can easily induce uneven Li deposition on the anode, which will cause drastic volume changes in the anode and repeated rupture/regeneration of the solid electrolyte interphase (SEI), resulting in a sharp drop in anode reversibility.[15−17] Finally, the accumulation of uneven Li deposition will induce the growth of Li dendrites, and Li dendrites may pierce the separator and pose a risk of short circuits and combustion in batteries.

Therefore, constructing a stable SEI on the LMA is an effective strategy to protect Li metal, slow down the interfacial side reaction, induce uniform Li deposition, and obtain a long-cycle lifespan in LMBs.[7,18,19] The SEI is derived from the chemical−electrochemical reactions between components in the electrolyte and Li metal. The large volume change during Li metal deposition/stripping will lead to repeated rupture/regeneration of SEI and the continuous evolution of components and structures, which is not conducive to the reversible deposition/stripping behavior of Li metal.[20,21] Therefore, SEI-forming additives such as FEC,[22,23] VC,[24,25] and $LiNO_3$[26,27] have been introduced into the electrolyte, which could preferentially react to generate an inorganic-rich SEI to stabilize the interfacial structure and achieve a highly reversible LMA.

Due to the reduction potential of FEC (1.4−1.6 V vs Li^+/Li) is more positive than conventional solvents (ethylene

Received: August 6, 2026
Revised: November 5, 2026
Accepted: November 6, 2026

ACS Publications © XXXX American Chemical Society

Downloaded from pubs.acs.org/jacsat/article-pdf/doi/10.1021/jacs.6c16437/69193451/jacs.6c16437.pdf by XIAMEN UNIV, Jinbao Zhao on 15 November 2026

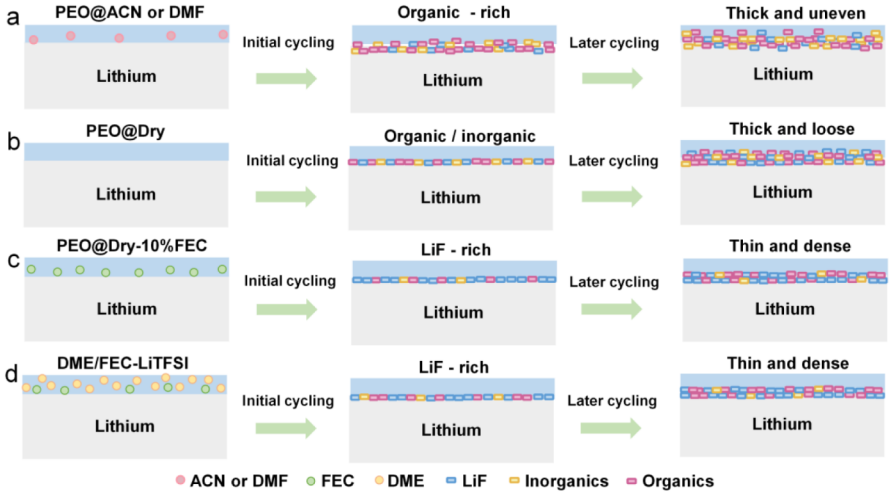

Figure 1. Schematic diagram of the interfacial evolution process of (a) PEO@ACN or PEO@DMF, (b) PEO@Dry, (c) PEO@Dry-10%FEC, and (d) DME@FEC electrolytes on the LMA.

carbonate, EC, 0.6−0.8 V vs Li^+/Li), it can preferentially decompose on the LMA to form an inorganic-rich SEI.[20,22] The main function of FEC is realized by producing the LiF component in the SEI, which can show significant advantages in battery cycling.[20,28] First, LiF has high interfacial energy and low solubility, which can effectively block the side reaction between electrolyte and Li metal. Second, the high ionic conductivity and low electron conductivity of LiF promote the uniform distribution of Li^+ ions and inhibit Li dendrite formation. Finally, the LiF-rich SEI has high mechanical strength, which can adapt to the volume changes during Li deposition/stripping, reduce the accumulation of "dead Li", and improve the Coulombic efficiency of the LMBs.[29] Although there are many studies of FEC into liquid electrolytes to improve the interfacial stability, the study of the interfacial reaction mechanism of FEC is difficult. Because the extremely strong reducing properties of Li metal will react with solvents, additives, anions, and other components, making that it is hard to study them.[30−32] Consequently, the interfacial behavior of a liquid electrolyte on the LMA reflects the collective outcome of multiple concurrent reactions. These intertwined chemical processes collectively govern the interfacial evolution of Li metal, complicating the identification of any single component's role. First, the multicomponent nature of the electrolyte complicates the study of FEC's intrinsic mechanism at the Li interface. Second, the SEI formed in such systems is a mosaic of products derived from free solvents, solvated species, and additives. It is a heterogeneous structure that fails to homogenize Li^+ flux and promotes dendrite growth. Third, parasitic interfacial reactions not only shape SEI evolution, but also generate various gaseous species,[33,34] which further perturb Li deposition and accelerate anode degradation. Taken together, these spontaneous chemical processes on the LMA surface constitute a major obstacle to deciphering the mechanistic role of any single additive and present a significant challenge for the targeted regulation of SEI composition. It is therefore essential to elucidate the interfacial chemistry of individual electrolyte components on the LMA. Such knowledge not only reveals the intrinsic reaction pathways of each species, but also informs the rational design of SEI composition and architecture.

PEO-based SPEs offer good interfacial compatibility with Li metal, owing to their high flexibility and chemical stability.[35−37] Importantly, they exhibit minimal parasitic reactions with Li and effectively immobilize anions through coordination with polymer segments, thereby limiting their continuous interaction with Li metal. These features make PEO-based SPEs an ideal model substrate for isolating the interfacial chemistry of FEC on the LMA.[38,39] Since PEO-based SPEs contain only PEO as the matrix and LiTFSI as the Li salt, the resulting SEI is mainly derived from the reductive decomposition of these two components, yielding a relatively simple SEI chemistry. This compositional simplicity makes PEO-based SPEs an attractive model substrate for investigating the interfacial reaction of additives such as FEC on the LMA. However, conventional wet-process SPEs are prepared by dissolving PEO and Li salts in solvents such as acetonitrile (ACN) or *N*,*N*-dimethylformamide (DMF),[40,41] followed by solvent evaporation (designated as PEO@ACN or PEO@DMF). This process often leaves residual polar solvent molecules, which can participate in the Li^+ solvation sheath and react with Li metal, thereby introducing additional interfacial complexity.[40,41] To avoid traditional liquid organic solvent-induced interfacial interference, we prepared a solvent-free dry-process PEO-based SPE (designated as PEO@Dry) using a simple and scalable heating-roller method. This system preserves the intrinsic interfacial reactions between PEO, LiTFSI, and Li metal but excludes the additional and competing reactions introduced by liquid solvents. FEC was then introduced into this PEO@Dry system to investigate its interfacial reaction mechanism on the LMA in the absence of solvent-derived complications. This work retains the intrinsic interfacial reactions between PEO and Li salts and constructs a controllable solvent-free PEO/LiTFSI substrate to eliminate additional interference from liquid solvents, thereby clarifying the interfacial reaction pathways of FEC and their impact on SEI formation and evolution.

However, the high crystallinity and low Li^+ transference number of PEO-based SPEs may alter the diffusion behavior, decomposition potential, and SEI formation pathway of FEC compared to liquid electrolytes. To isolate the intrinsic chemical effect of FEC from the influence of the PEO matrix, we constructed a liquid electrolyte control system with a

Downloaded from pubs.acs.org/jacsat/article-pdf/doi/10.1021/jacs.6c16437/6919345/jacs.6c16437.pdf by XIAMEN UNIV. Jinbao Zhao on 15 November 2026

https://doi.org/10.1021/jacs.6c16437
J. Am. Chem. Soc. XXXX, XXX, XXX−XXX

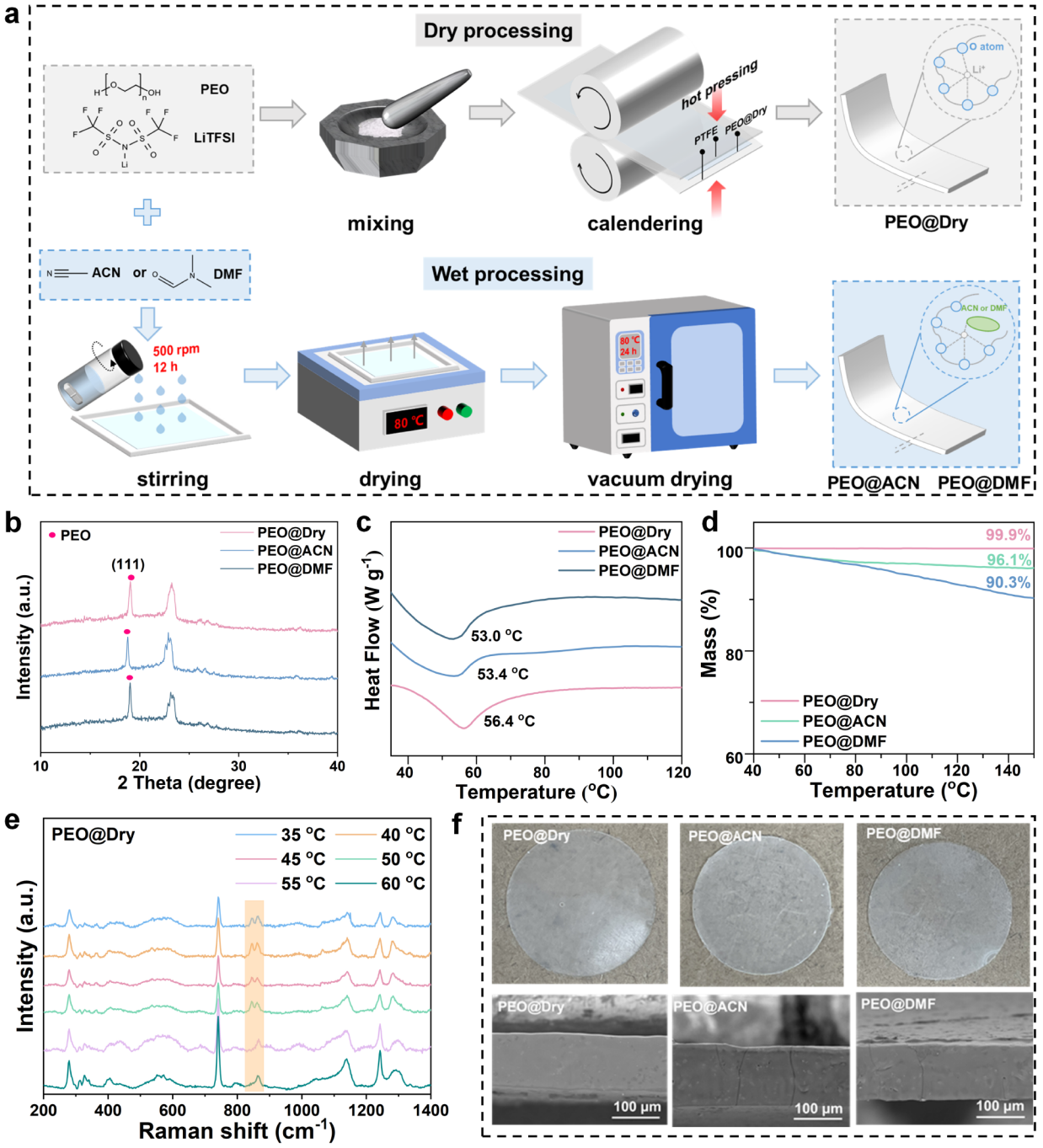

Figure 2. (a) Schematic diagram of PEO-based SPEs prepared by dry and wet processes. (b) XRD spectra, (c) DSC, and (d) TG curves of PEO@Dry, PEO@ACN, and PEO@DMF. (e) Raman spectra of PEO@Dry from 35 to 60 °C. (f) Optical photographs and cross-section SEM images of PEO@Dry, PEO@ACN, and PEO@DMF.

similar chemical composition but fundamentally different transport environments. Glyme (DME) was chosen as the liquid analogue as it shares the same ether-based chemistry as PEO, offering comparable polarity and solvation characteristics. A DME-LiTFSI solution with a Li−O ratio of 18 was prepared as the liquid counterpart to PEO@Dry, and 10 wt % FEC was added to this solution (designated as DME@FEC) as the control for PEO@Dry-10%FEC.

Herein, our results reveal that FEC undergoes both chemical and electrochemical reactions on the LMA, with the latter proceeding at a significantly faster rate. The introduction of FEC can effectively modulate the composition and structure of the SEI. The SEI evolution of the four electrolytes is according to the following process. In wet-processed SPEs (PEO@ACN or PEO@DMF), residual solvents such as ACN or DMF react with Li metal, interfering with SEI formation and leading to an organic-rich SEI in the initial cycles. Extensive side reactions cause rapid SEI thickening, and the accumulated organic layer progressively impedes Li^+ conduction, inducing uneven Li deposition and accelerating the repeated rupture and regeneration of the SEI (Figure 1a). In contrast, the solvent-free PEO@Dry yields an SEI derived solely from the decomposition of PEO and LiTFSI, forming a hybrid organic−inorganic structure. Upon prolonged cycling, this

https://doi.org/10.1021/jacs.6c16437
J. Am. Chem. Soc. XXXX, XXX, XXX−XXX

Downloaded from pubs.acs.org/jacsat/article-pdf/doi/10.1021/jacs.6c16437/6919345 1/jacs.6c16437.pdf by XIAMEN UNIV., Jinbao Zhao on 15 November 2026

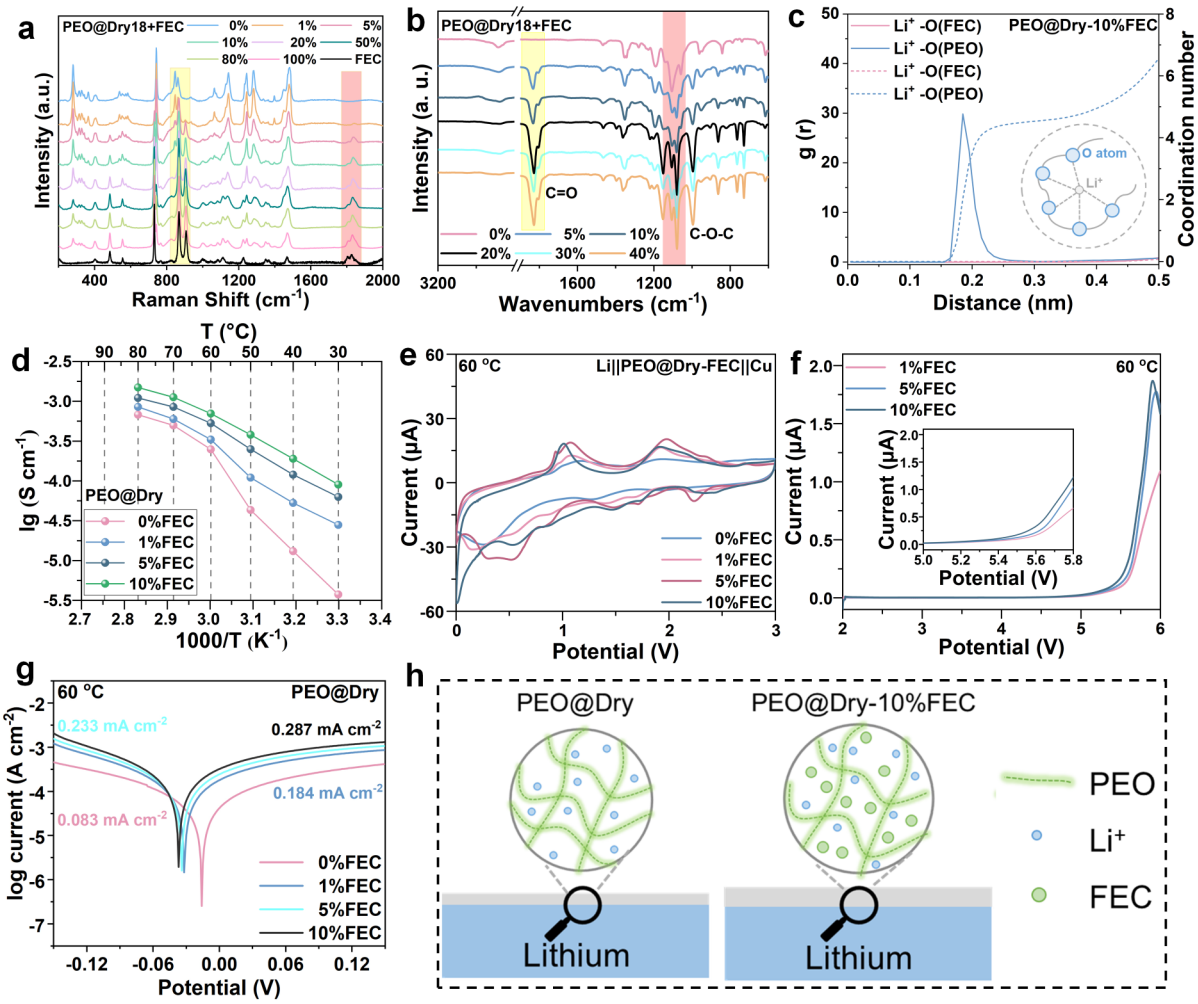

Figure 3. (a) Raman and (b) FTIR spectra of PEO@Dry with different FEC. (c) RDF results of the radial distribution function of PEO@Dry-10% FEC. (d) Variable-temperature ionic conductivity, (e) CV, (f) LSV, and (g) Tafel curves of PEO@Dry with FEC. (h) Schematic diagram of the structure of PEO@Dry and PEO@Dry with FEC.

SEI continues to thicken and develops a porous morphology (Figure 1b). When FEC is introduced into PEO@Dry (PEO@Dry-10%FEC), it preferentially reacts with Li metal to form a LiF-rich SEI. The LiF component facilitates fast Li^+ transport, enhances interfacial ion transfer, and promotes uniform Li deposition, which in turn sustains a thin and dense SEI during cycling (Figure 1c). A similar effect is observed in the liquid analogue DME@FEC: the LiF-rich SEI effectively passivates the anode interface, suppressing the reductive decomposition of LiTFSI and DME, and minimizing byproduct formation (Figure 1d). This LiF-rich interface also improves Li^+ transport and promotes uniform deposition. Importantly, the underlying mechanism of FEC is found to be consistent across the solid and liquid electrolytes. The performance differences between the two systems arise primarily from variations in FEC mobility, transport kinetics, and reaction rates, rather than from any fundamental change in its film-forming chemistry. This comparative approach, combining solid-state and liquid-phase model systems, offers an innovative perspective for deconvoluting the interfacial chemistry of individual electrolyte components on the LMAs.

RESULTS AND DISCUSSION

Comparison of Dry-Processed and Wet-Processed PEO-SPEs

PEO-based SPEs exhibit good compatibility with Li metal, making them a suitable model substrate for investigating interfacial chemistry on the LMA. However, conventional wet-process SPEs often retain residual solvent, which may participate in the interfacial reaction and complicate the mechanistic analysis. To eliminate such interference, we prepared a solvent-free PEO-based SPE via a dry-process route (PEO@Dry, Figure 2a). Optical and SEM images confirm that this method yields complete and dense electrolyte membranes (Figure 2f). XRD spectra and DSC curves indicate that PEO@Dry shares the same crystalline structure with the wet-process electrolyte (Figure 2b) but with a higher degree of crystallinity (Figure 2c). TG measurements show distinct mass losses of 3.9% for PEO@ACN and 9.7% for PEO@DMF, corresponding to the evaporation of residual ACN and DMF solvents, respectively (Figure 2d). Variable-temperature Raman spectra reveal that the chelation peak between the ether-oxygen (EO) chain segment and Li^+ ions at 863 cm^{-1} of PEO@Dry persists to the highest temperature in PEO@Dry compared with the wet-processed electrolytes (Figures 2e and

Downloaded from pubs.acs.org/jacsat/article-pdf/doi/10.1021/jacs.6c16437/6919345/jacs.6c16437.pdf by XIAMEN UNIV. Jinbao Zhao on 15 November 2026

https://doi.org/10.1021/jacs.6c16437
J. Am. Chem. Soc. XXXX, XXX, XXX−XXX

S1), indicating that the crystalline domains of PEO@Dry vanish last upon heating. Electrochemical measurements show that both the ionic conductivity (Figure S2) and Li^+ transference number (Figure S3) of PEO@Dry are lower than those of PEO@ACN and PEO@DMF. The improved conductivity in the wet-processed systems is likely due to the plasticizing effect of residual solvents, which reduce PEO crystallinity and facilitate ion migration. PEO@Dry, by contrast, contains no residual solvents, which accounts for its higher crystallinity and consequently lower ionic conductivity and Li^+ ion transference number. FTIR spectra of PEO@DMF show a characteristic peak at 676 cm^{-1} (Figure S4), which is assigned to the interaction between DMF and Li^+, indicating that residual DMF molecules participate in the Li^+ solvation sheath. These strongly polar solvent residues are thus expected not only to affect ion conduction but also to interfere with the interfacial chemistry at the Li metal surface. Cyclic voltammetry (CV) tests were performed in Li||SPEs||Cu half-cells to probe the extent of interfacial reactions between the various electrolytes with Li metal. In the CV profiles, the Li|| PEO@Dry||Cu cell displays only two well-defined reduction peaks (Figure S5a). In contrast, the PEO@ACN and PEO@ DMF cells show a notably greater number of reduction features (Figure S5b,c), suggesting that residual solvents in the wet-processed electrolytes trigger additional side reactions at the Li interface. And symmetrical cells with different electrolytes were assembled to monitor the evolution of Li metal. Optical images reveal that the LMA degrades more severely in PEO@ACN and PEO@DMF than in PEO@Dry (Figure S6). SEM analysis further shows that, after 100 cycles, the LMA in PEO@Dry exhibits significant byproduct accumulation; in contrast, uneven deposition and dead Li are already evident after only 50 cycles in PEO@ACN and PEO@ DMF (Figure S7). This contrast underscores that the solvent-free PEO@Dry effectively suppresses parasitic reactions at the LMA, yielding a more stable electrode/electrolyte interface. Collectively, PEO@Dry eliminates the interference of residual solvents inherent to wet processing, and thus serves as an ideal model substrate for investigating the interfacial evolution of LMAs.

Interaction between FEC and Electrolyte

PEO@Dry is therefore used as a model system to probe the interfacial chemistry of FEC on the LMA. It is necessary to verify that FEC acts predominantly at the interface rather than interacting preferentially with LiTFSI or the PEO matrix. Raman spectroscopy is employed to probe the interaction between FEC and the PEO-Li^+ coordination environment. As the FEC content increases, the 863 cm^{-1} peak (EO-Li^+ chelation) remains essentially unshifted (Figures 3a and S8), suggesting that FEC does not competitively coordinate with Li^+ to an appreciable extent within the PEO matrix at an O/Li ratio of 18. FTIR spectra show that, as the FEC content increases, the 1106 cm^{-1} peak (EO segment) position remains essentially unchanged, whereas the C═O peak (1835 cm^{-1}) intensity progressively increases (Figures 3b and S9). Additionally, the EO vibration shows no significant shift with varying Li salt content (i.e., different O/Li ratios), further confirming the absence of detectable interaction between FEC and the PEO matrix. A closer inspection of the FTIR spectra reveals that, as the FEC content increases, the EO vibration peaks begin to split (Figure S10), implying the coexistence of different phase states of PEO. This observation suggests that the introduction of FEC perturbs the local ordering of PEO chains, thereby affecting the crystallinity of the electrolyte. Radial distribution function (RDF) calculation results for the PEO@Dry-10%FEC further confirm that Li^+ ions are predominantly coordinated by the O atoms of the PEO segments, whereas the O atoms of FEC are scarcely involved in Li^+ coordination (Figure 3c). These results indicate that FEC does not significantly interact with Li^+ in the bulk PEO electrolyte but instead participates primarily in interfacial reactions with Li metal, where free FEC molecules are reduced chemically and electrochemically at the LMA surface and incorporated into the SEI. This is attributable to the strong chelation of Li^+ by the EO segments in the PEO18 system, which firmly confines Li^+ within the polymer matrix.

We next examined the influence of the FEC content on the bulk transport properties of PEO@Dry. The ionic conductivity, measured as a function of temperature, increases with increasing FEC addition (Figure 3d). Likewise, the Li^+ transference number exhibits a corresponding enhancement (Figure S11), suggesting that FEC facilitates ion transport within the PEO matrix. The FEC swells the PEO matrix and lowers its crystallinity, as made evident by the FTIR results. This structural modification reduces the binding strength between EO segments and Li^+, leading to an improved Li^+ mobility and higher ionic conductivity. The CV curves of Li|| PEO@Dry||Cu cells show only two pairs of reversible redox peaks, corresponding to Li deposition/stripping and electrolyte decomposition, respectively (Figure S12a). Upon FEC addition, the oxidation branch remains largely unchanged, whereas the reduction branch develops multiple irreversible peaks, the number of which increases with the FEC content (Figures 3e and S12). This indicates that FEC readily participates in interfacial reactions with the Li metal during the cathodic scan. Consistent with this, LSV tests reveal that FEC narrows the electrochemical stability window of the electrolyte (Figure 3f), suggesting that the reductive decomposition of the electrolyte is promoted by the interfacial activity of FEC. Tafel analysis shows that the exchange current density increases with FEC addition, accompanied by a negative shift in the corrosion potential and accelerated anode interfacial kinetics (Figures 3g and S13). Collectively, the physical and electrochemical characterizations indicate that FEC does not significantly interact with LiTFSI or the PEO matrix in the bulk phase. Instead, its primary effects are 2-fold: (i) swelling the PEO matrix to facilitate ion transport, and (ii) participating in interfacial reactions to influence SEI formation and anode stability (Figure 3h).

Gas Production Behavior of Electrolytes

To gain insight into the interfacial reactions of FEC on the LMA, we performed differential electrochemical mass spectrometry (DEMS) to track the gas species evolved during electrochemical cycling. H_2 acts as a gaseous signal for interfacial reactions, which can reflect the dynamic changes in chemical and electrochemical reactions for the PEO@Dry−FEC system. The H_2 production behavior of batteries is indeed a very complex process, which can be regarded as a macroscopic manifestation of various interfacial reactions.[43,44] Under high-temperature conditions, chemical reactions between FEC and Li metal, along with subsequent interfacial side reactions, may result in H_2 production.[45] The gas evolution profiles directly reflect the chemical and electrochemical decomposition pathways of FEC at the anode

Downloaded from pubs.acs.org/jacsat/article-pdf/doi/10.1021/jacs.6c16437/6919345/jacs.6c16437.pdf by XIAMEN UNIV. Jinbao Zhao on 15 November 2026

https://doi.org/10.1021/jacs.6c16437
J. Am. Chem. Soc. XXXX, XXX, XXX−XXX

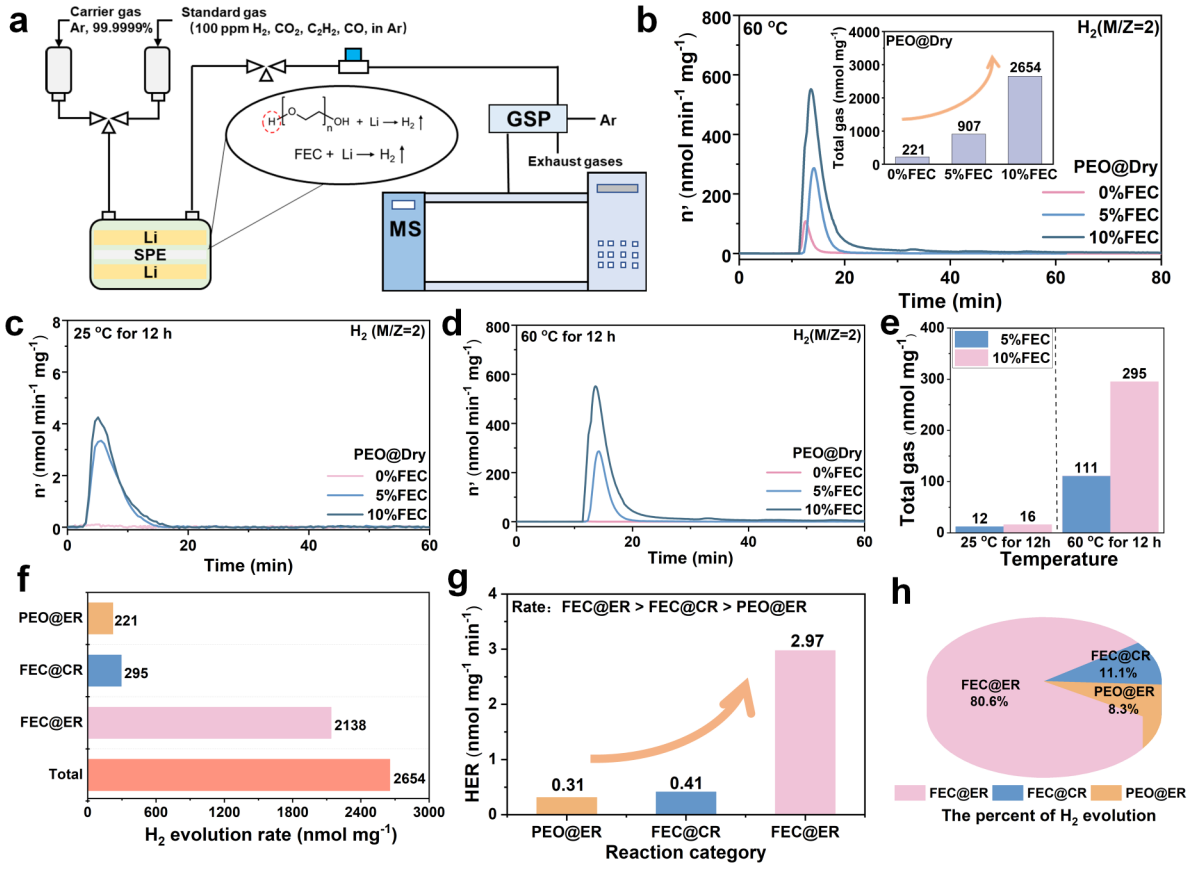

Figure 4. (a) Schematic diagram of DEMS testing. (b) H_2 generation curves in PEO@Dry electrolytes with different amounts of FEC in Li||SPEs|| Li symmetrical cells after cycling for 12 h at 60 °C. H_2 generation curves in PEO@Dry with different amounts of FEC in Li||SPEs||Li symmetrical cells at (c) 25 °C and (d) 60 °C for 12 h. (e) H_2 production in PEO@Dry with different amounts of FEC in Li||SPE||Li symmetrical batteries at 25 and 60 °C for 12 h. (f) Total H_2 production, (g) H_2 production rate, and (h) H_2 production proportion for various interfacial reactions.

interface (Figure 4a). To deconvolute the chemical and electrochemical contributions of FEC at the LMA interface, we monitored the evolution rate and cumulative production of H_2. In PEO@Dry-10%FEC system, three potential reactions may generate H_2: (i) electrochemical decomposition of PEO (designated as PEO@ER), (ii) chemical reaction between FEC and Li metal (designated as FEC@CR), and (iii) electrochemical reduction of FEC (designated as FEC@ER). To deconvolute the H_2 evolution pathways, we first examined the chemical reactivity of FEC with Li metal under open-circuit conditions. PEO itself shows negligible H_2 production, consistent with its limited number of terminal −OH groups and low polarity. In contrast, FEC reacts spontaneously with Li metal to generate H_2, and the amount of H_2 increases with FEC content (Figure 4c,d). After 12 h of resting at 25 °C, the H_2 production for PEO@Dry-5%FEC and PEO@Dry-10% FEC are 12 and 16 nmol mg^{-1}, respectively; these values rose to 111 and 295 nmol mg^{-1} at 60 °C (Figure 4e). These results confirm that H_2 generation during resting originates primarily from the spontaneous chemical reaction between FEC and Li metal, while PEO itself remains essentially inert. Upon electrochemical cycling, H_2 evolution accelerates markedly (Figure 4b). From PEO@Dry to PEO@Dry-10%FEC, the total H_2 production surges from 221 to 2,654 nmol mg^{-1}, and the H_2 generation rate increases sharply with FEC content, indicating that the electrochemical reduction of FEC (FEC@ ER) proceeds significantly faster than that of PEO (PEO@ ER). To quantify the individual contributions, we subtracted the H_2 yields of PEO@ER and FEC@CR from the total production. The resulting H_2 amounts for PEO@ER, FEC@ CR, and FEC@ER are 221, 295, and 2,138 nmol mg^{-1}, respectively (Figure 4f), corresponding to production rates of 0.31, 0.41, and 2.97 nmol mg^{-1} min^{-1} (Figure 4g), and accounting for 8.3%, 11.1%, and 80.6% of the total H_2 evolution, respectively (Figure 4h). These results demonstrate that (i) the chemical reaction between FEC and Li metal persists during cycling; (ii) the electrochemical reaction dominates H_2 generation, owing to current-driven enhancement; and (iii) FEC@ER is the primary source of H_2 during battery operation, underscoring the significant impact of FEC on the interfacial chemistry of the LMA. Among the above H_2 production results, the comparison between 5% and 10% FEC is mainly used to examine the relationship between H_2 production behavior and the addition of FEC. In practice, when 5% FEC is added, the amount of FEC can involve in interfacial reaction is limited, resulting in weaker interfacial regulation. And 10% FEC addition can produce stable and repeatable interfacial reactions without significantly affecting ion transport and the underlying structure of PEO substrate. But infinite FEC may complicate interface responses and SEI evolution. Therefore, considering the controllability of mechanism analysis, 10% FEC is selected as a representative addition for in-depth study. Combined with previous conclusions that FEC does not participate in Li^+ solvation structures, it can be inferred that the interfacial reaction follows a sequential process in which FEC first undergoes chemical

https://doi.org/10.1021/jacs.6c16437
J. Am. Chem. Soc. XXXX, XXX, XXX−XXX

Downloaded from pubs.acs.org/jacsat/article-pdf/doi/10.1021/jacs.6c16437/69193451/jacs.6c16437.pdf by XIAMEN UNIV, Jinbao Zhao on 15 November 2026

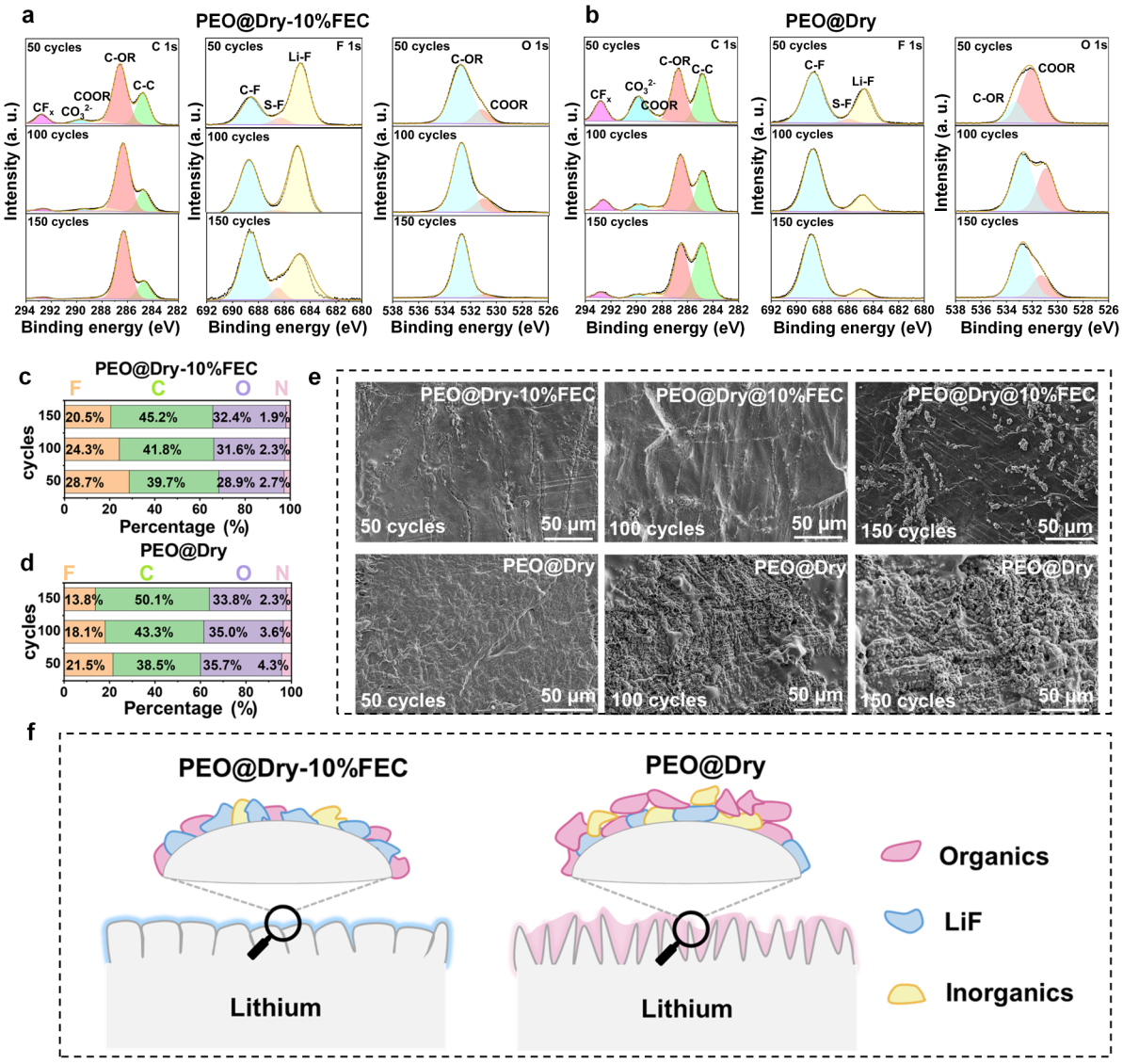

Figure 5. XPS spectra of LMA after different cycles in (a) PEO@Dry-10%FEC and (b) PEO@Dry. The elemental distribution of SEI after different cycles in (c) PEO@Dry-10%FEC and (d) PEO@Dry. (e) SEM images of LMA after different cycles for PEO@Dry-10%FEC and PEO@Dry. (f) Schematic diagram of the SEI composition of LMA after different cycles in PEO@Dry-10%FEC and PEO@Dry.

reactions during the resting stage and is subsequently electrochemically reduced during battery operation, accompanied by only limited decomposition of PEO. Accordingly, SEI formation is dominated by the chemical and electrochemical conversion of FEC, while the decomposition of PEO makes only a minor contribution. This sequential, multistep interfacial reaction mechanism determines the composition and structure of the SEI and influences the evolution process of SEI. Specifically, the initial chemical reaction preforms a LiF-rich inorganic framework that acts as a nucleation layer, while the subsequent electrochemical reduction of FEC further reinforces this framework with additional LiF and organic components, leading to a stable and passivating SEI with minimal PEO-derived contamination.

Evolution of LMA after the Introduction of FEC into PEO@Dry

The dominant H_2 evolution from FEC@ER (80.6%) suggests that FEC is extensively reduced at the LMA interface during cycling, implying its direct involvement in SEI construction. To elucidate the compositional evolution of the SEI, we performed X-ray photoelectron spectroscopy (XPS) on Li anodes after storage at 25 and 60 °C for various durations. For PEO@Dry, the relative contents of $-CF_x$ and LiF show only a slight increase at 25 °C over time, while the other components remain essentially unchanged (Figure S14). At 60 °C, the growth rates of $-CF_x$ and LiF are accelerated, yet the overall chemical structure of the SEI still exhibits no significant variation (Figure S15). These observations indicate that, in the absence of FEC, PEO@Dry and Li metal undergo minimal direct reaction; the minor compositional changes are attributed to the slow reductive decomposition of $TFSI^-$, which is limited in extent and highly dependent on temperature and aging time. In contrast, for PEO@Dry-10%FEC, the LiF content increases steadily even at 25 °C (Figure S16). At 60 °C, the initial LiF content is already high and further rises rapidly with prolonged resting time (Figure S17), confirming the pronounced reactivity of FEC with Li metal and its dominant role in constructing a LiF-enriched SEI. Quantitative elemental analysis of the SEI (Figure S18) shows that PEO@Dry-10%

https://doi.org/10.1021/jacs.6c16437
J. Am. Chem. Soc. XXXX, XXX, XXX−XXX

Downloaded from pubs.acs.org/jacsat/article-pdf/doi/10.1021/jacs.6c16437/6919345 1/jacs.6c16437.pdf by XIAMEN UNIV, Jinbao Zhao on 15 November 2026

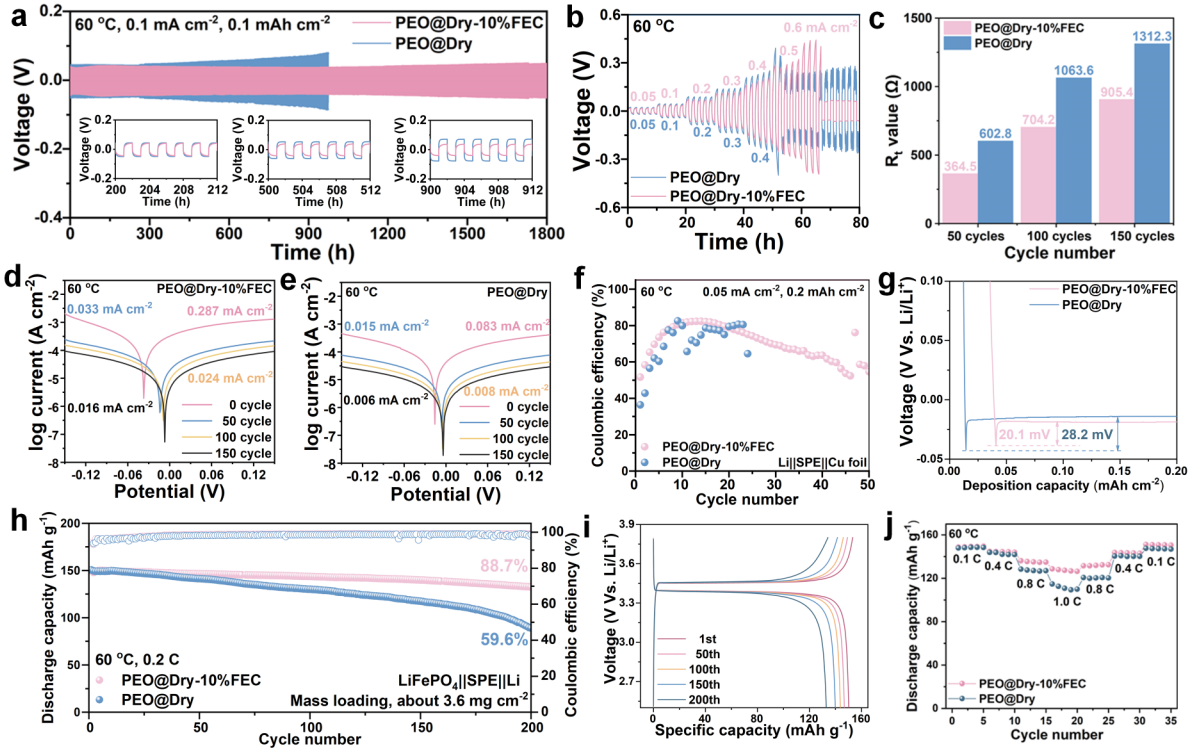

Figure 6. (a) The time-voltage curves of Li||SPE||Li cells at 60 °C with 0.1 mA cm^{-2}, 0.1 mA h cm^{-2}. (b) The CCD plots of PEO@Dry and PEO@Dry-10%FEC. (c) The value of R_t of symmetrical cell after different cycles in PEO@Dry-10%FEC and PEO@Dry. Tafel curves of symmetrical cell in (d) PEO@Dry-10%FEC and (e) PEO@Dry after different cycles at 60 °C. (f) The Coulombic efficiency and (g) the initial Li plating curves of Li||SPE||Cu cells at 60 °C with 0.05 mA cm^{-2}, 0.2 mA h cm^{-2}. (h) The performance of PEO@Dry-10%FEC and PEO@Dry with $LiFePO_4$ cathode at a 0.2 C rate at 60 °C. (i) The voltage profiles of PEO@Dry-10%FEC and at the rate of 0.2 C at different cycles. (j) Rate performance of LFP|| SPE||Li cells with PEO@Dry-10%FEC and PEO@Dry.

FEC exhibits a persistently high F content with a steady increase over time, in marked contrast to PEO@Dry, where both the F increment and its growth rate are significantly lower. This striking difference demonstrates that FEC preferentially reacts with Li metal to form a dense, LiF-rich SEI, which acts as a stable passivation layer and structural framework for subsequent interfacial evolution. By effectively suppressing continuous electrolyte decomposition, this inorganic-rich framework promotes the formation of a thinner and more stable SEI. In contrast, the FEC-free PEO@Dry electrolyte lacks such an inorganic scaffold, resulting in continuous SEI reconstruction, sustained electrolyte consumption, and progressive interphase thickening during cycling. Notably, the interfacial reaction pathway of FEC is governed by its solvation state. In conventional liquid electrolytes, FEC partially enters the Li^+ solvation sheath and undergoes electrochemical reduction together with other electrolyte components, producing a mixed organic/inorganic SEI. By contrast, in the solvent-free PEO@Dry electrolyte, FEC remains uncoordinated with Li^+ and undergoes spontaneous chemical reduction before electrochemical reduction, yielding a sequential chemical-electrochemical pathway that constructs a compact, LiF-rich SEI. These findings identify Li^+−FEC coordination as the key factor governing interfacial reaction pathways and SEI evolution.

SEM images reveal that the LMA surface in the PEO@Dry-10%FEC remains flat and free of visible byproduct deposition throughout the resting period, owing to the protective SEI layer (Figure S19a−c). In contrast, for PEO@Dry, the continuous reductive decomposition of $TFSI^-$ leads to progressive accumulation of byproducts on the LMA with increasing resting time, resulting in a rough and uneven surface (Figure S19d−f). The EIS measurements are used to monitor the interfacial transport resistance (R_t) of Li^+. The PEO@Dry-10%FEC maintains a low R_t with only a slight increase over time: after 12, 24, and 48 h of resting at 60 °C, the R_t values are 160.5, 178.6, and 197.2 Ω, respectively (Figure S20a), indicating excellent interfacial stability. By contrast, the PEO@Dry shows R_t values of 309.3, 349.5, and 371.1 Ω under the same conditions (Figure S20b), reflecting continuous deterioration of the anode interface.

To further track the consumption of electrolyte components during cycling, we disassembled the symmetrical cells after different cycle numbers and characterized the electrolytes by FTIR and Raman spectroscopy. FTIR spectra show that the C═O peak of FEC at 1735 cm^{-1} gradually weakens with cycling (Figure S21), indicating that FEC is continuously consumed through its participation in SEI formation. Raman spectra reveal that the crystallization peak of PEO at 844 cm^{-1} increases in intensity upon cycling, suggesting that both FEC and Li salts are consumed, leading to increased PEO crystallinity. Notably, the crystallization peak intensifies more significantly for PEO@Dry-10%FEC than for PEO@Dry (Figure S22), confirming that FEC participates more extensively in the interfacial reactions with Li metal than LiTFSI does. Collectively, these results demonstrate that FEC constructs a LiF-rich, dense SEI on the LMA through a "chemical self-sacrifice" mechanism. This SEI effectively suppresses parasitic side reactions, preserves interfacial stability, and ensures the long-term static stability of the LMA.

https://doi.org/10.1021/jacs.6c16437
J. Am. Chem. Soc. XXXX, XXX, XXX−XXX

Downloaded from pubs.acs.org/jacsat/article-pdf/doi/10.1021/jacs.6c16437/6919345/jacs.6c16437.pdf by XIAMEN UNIV. Jinbao Zhao on 15 November 2026

The evolution of the LMA after cycling is investigated using Li||Li symmetrical cells with different electrolytes at 60 °C, with the aim of revealing the interfacial reaction mechanisms of FEC on the anode during electrochemical cycling. XPS results show that in PEO@Dry-10%FEC, the LiF content decreases gradually but the SEI composition remains generally stable upon cycling (Figure 5a). In contrast, the SEI in PEO@Dry undergoes continuous compositional changes (Figure 5b), reflecting repeated rupture and regeneration without achieving structural stability. Quantitative F analysis further confirms that the F content in PEO@Dry-10%FEC stays high in the early cycles and then declines gradually from 28.7% after 50 cycles to 24.3% after 100 cycles and 20.5% after 150 cycles (Figure 5c), whereas that in PEO@Dry remains persistently low (Figure 5d). This behavior is attributed to the preferential reaction of FEC with Li metal, which forms a LiF-rich SEI framework during the initial stage and accounts for the high F content. Although FEC is gradually depleted and its replenishment is restricted by the PEO matrix, resulting in a slight decline in LiF content upon prolonged cycling, the initially formed LiF-rich framework remains structurally intact. Owing to its high Li^+ conductivity and mechanical robustness, this inorganic backbone provides persistent ion-transport pathways and mechanical support, thereby suppressing continuous electrolyte decomposition and maintaining interfacial stability. Consequently, subsequent SEI growth is dominated by organic species that reinforce the inorganic framework without compromising its integrity. SEM observations further confirm that the PEO@Dry-10%FEC electrode maintains a smooth surface with uniform Li deposition and negligible byproduct accumulation throughout cycling (Figure 5e). In contrast, the FEC-free PEO@Dry electrolyte forms a fragile organic/inorganic mosaic SEI that undergoes repeated rupture and regeneration, leading to severe byproduct accumulation, progressive SEI thickening, and nonuniform Li deposition. These results demonstrate that the early formation of a LiF-rich framework governs subsequent SEI evolution and is essential for stabilizing the Li metal interface (Figure 5f). The persistent evolution of its structure and composition reflects ongoing interfacial side reactions, which not only accelerate LMA deterioration but also impede Li^+ transport, promote uneven Li deposition and "dead-Li" formation, and severely compromise the cycling stability of LMBs.

Electrochemical Properties of PEO@Dry-FEC

To assess the long-term cycling stability of the electrolytes, we conducted galvanostatic cycling tests on Li||Li symmetrical cells and Li||$LiFePO_4$ (LFP) half-cells. At 60 °C, the Li||PEO@Dry-10%FEC||Li symmetrical cell achieves a stable cycling duration of 1800 h at 0.1 mA cm^{-2} with 0.1 mA h cm^{-2}, accompanied by a low and stable polarization overpotential. Meanwhile, the FEC-free PEO@Dry cell fails after only 950 h under the same conditions (Figure 6a). The critical current density (CCD), defined as the maximum tolerable current density, serves as a key indicator of the electrolyte's resistance to dendrite formation.[42] Potential oscillations at elevated current densities reflect interfacial instability arising from uneven Li^+ flux. The CCD of the PEO@Dry-10% FEC is 0.6 mA cm^{-2}, significantly higher than the 0.4 mA cm^{-2} observed for PEO@Dry (Figure 6b), demonstrating that FEC promotes interfacial ion transport and effectively mitigates dendrite growth. The R_t value is defined as interfacial transfer resistance, which includes SEI resistance and charge-transport resistance, used to characterize the interfacial reaction resistance of Li^+ during charge transfer at the electrode/electrolyte interface, and also serves as a performance indicator for Li^+ transport to SEI. A lower R_t facilitates rapid Li^+ transport to the anode surface, thereby promoting uniform Li deposition and inhibiting dendrite growth. Upon cycling, the R_t of the Li||PEO@Dry-10%FEC||Li symmetrical cell is increased from 364.5 Ω, 704.2 Ω to 905.4 Ω (Figures 6c and S23a). By contrast, the R_t values for the PEO@Dry cell are 602.8 Ω, 1063.6 Ω, and 1312.3 Ω after the same cycle numbers (Figure S23b), confirming that FEC effectively maintains a stable and low-resistance interface during prolonged cycling. The difference in interfacial transport performance is also reflected in the deposition behavior and morphological evolution of LMA. An unstable SEI tends to accumulate and thicken upon cycling, leading to an increase in R_t and a higher energy barrier for Li^+ transport across the interface. The Tafel curves of symmetrical batteries after different cycles show that the exchange current density (J_a) decreases from 0.287 mA cm^{-2} to 0.016 mA cm^{-2} after 150 cycles, and the corrosion potential is shifted positively by 30 mV (Figure 6d,e). This indicates that the SEI constructed by FEC can effectively slow down the interfacial side reactions, maintain structural stability, and continuously protect LMA during cycling. In addition, Li||PEO@Dry-10% FEC||Li also performed a stable cycle of 450 h at 25 °C (Figure S24). This is due to that the FEC improved the ionic conductivity of electrolyte, allowing batteries to achieve a lower polarization potential and reversible cycling at room temperature. Meanwhile, FEC would induce the formation of stable LiF-rich SEI on the anode, which could effectively passivate Li metal and inhibit interfacial side reactions while improving Li^+ ions conductivity in the SEI, so that the LMA could expressed excellent cyclic stability.

Meanwhile, since FEC has effectively regulated the deposition behavior of Li metal, Li||PEO@Dry-10%FEC||Cu half-cell achieved a stable cycle of about 50 cycles (Figure 6f) and shows a lower nucleation overpotential of Li metal (Figure 6g). However, Li||PEO@Dry||Cu half-cell could hardly work effectively at 60 °C. The capacity retention of LFP||PEO@Dry-10%FEC||Li half-cell is 88.7% after 200 cycles at 0.2 C, showing considerable electrochemical performance (Figure 6h,i). However, LFP||PEO@Dry||Li half-cell appeared to have a significant capacity decay trend after only 60 cycles. Moreover, LFP||PEO@Dry-10%FEC||Li half-cell could stably keep 200 cycles with a capacity retention rate of 75.1% at 0.4 C (Figure S25). And the cells also show better rate performance (Figure 6j). In the same way, the addition of FEC effectively improves the Li^+ ions transport performance of the SEI, promotes uniform Li deposition, inhibits Li dendrite growth and dead Li formation, and increases the cycling stability of LMA. And FEC formed a SEI with clear composition and stable structure on the Li metal surface, which effectively protected Li metal. The organic−inorganic SEI with good toughness could effectively overcome the huge volume expansion of LMA during the charging and discharging processes and improve the cycle reversibility of the anode.

Comparison Results with Liquid Electrolytes

The above results demonstrate that the addition of FEC to PEO@Dry effectively enhances both interfacial stability and electrochemical performance. To verify whether this mechanism is transferable to liquid systems, we constructed a liquid analogue using DME, which, like PEO, belongs to the ether

Downloaded from pubs.acs.org/jacsat/article-pdf/doi/10.1021/jacs.6c16437/6919345/jacs.6c16437.pdf by XIAMEN UNIV, Jinbao Zhao on 15 November 2026

https://doi.org/10.1021/jacs.6c16437
J. Am. Chem. Soc. XXXX, XXX, XXX−XXX

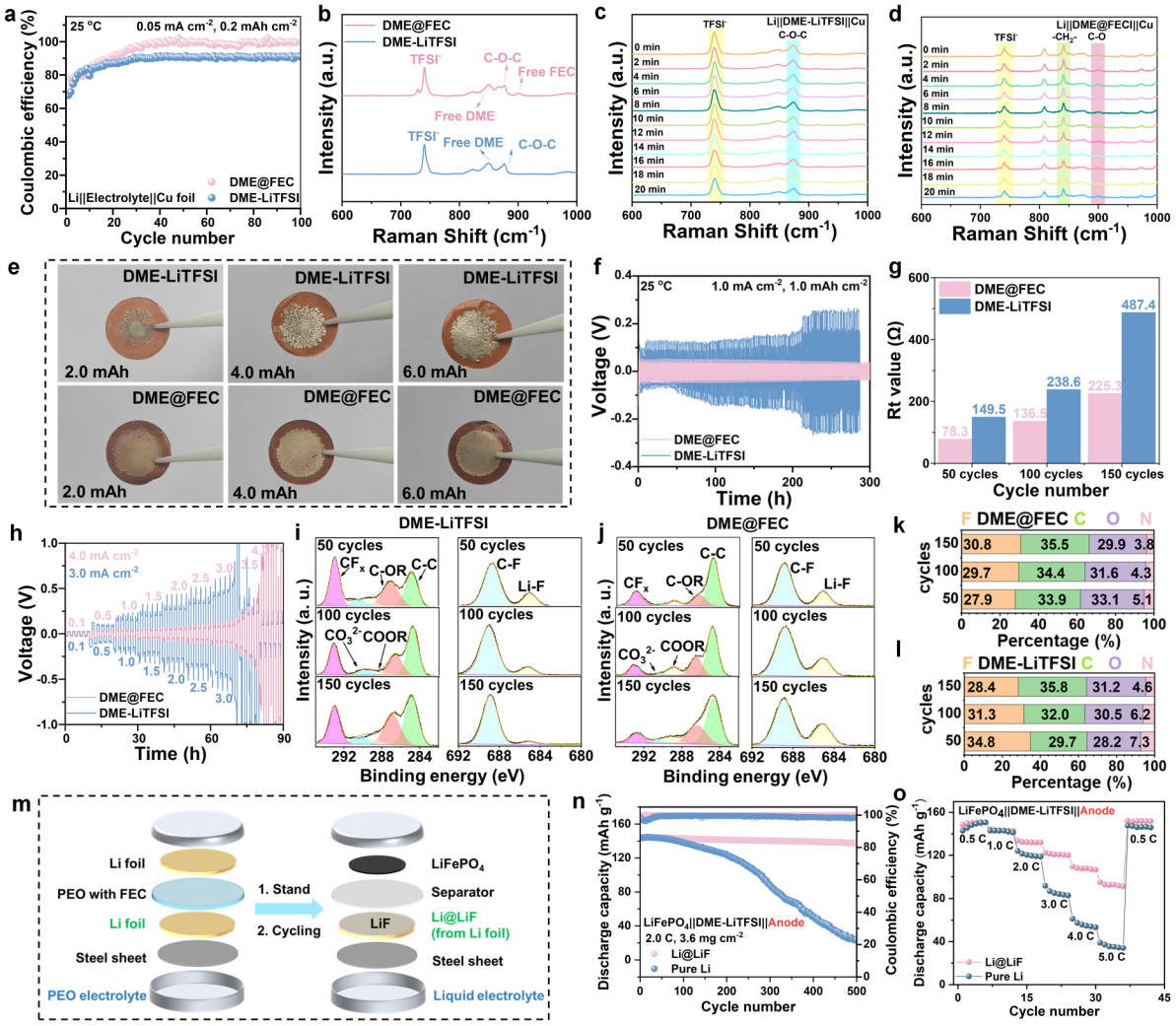

Figure 7. (a) The Coulombic efficiency of Li||Electrolytes||Cu half-cells at 25 °C with 0.05 mA cm^{-2}, 0.2 mA h cm^{-2}. (b) Raman spectra of DME-LiTFSI and DME@FEC electrolytes. Interfacial in situ Raman spectra of (c) DME-LiTFSI and (d) DME@FEC at a current density of 0.5 mA cm^{-2}. (e) Optical photographs of depositing different capacities of Li metal on Cu foil under different electrolytes. (f) The time-voltage curves of Li||Electrolytes||Li cells at 25 °C with 1.0 mA cm^{-2}, 1.0 mA h cm^{-2}. (g) The value of R_t of the symmetrical cell after different cycles in DME@FEC and DME-LiTFSI electrolytes. (h) The CCD plots of DME@FEC and DME-LiTFSI. XPS spectra of LMA after cycling in (i) DME-LiTFSI and (j) DME@FEC. The elemental distribution of SEI after cycling in (k) DME@FEC and (l) DME-LiTFSI. (m) Schematic diagram of assembling LFP||DME-LiTFSI||Anode (Li@LiF) cells. (n) The cycling performance of LFP||DME-LiTFSI||Anode at a 2.0 C rate. (o) Rate performance of LFP||DME-LiTFSI||Anode cells.

family and shares comparable polarity and solvation characteristics. A DME-LiTFSI solution is prepared as the liquid counterpart to PEO@Dry, and 10 wt % FEC is added (designated as DME@FEC) to serve as the control for PEO@Dry-10%FEC. The cycling results of Li||Cu half-cells show that DME@FEC performed a better cycle stability and higher Coulombic efficiency than the FEC-free DME-LiTFSI electrolyte (Figure 7a). The optical pictures of Li deposited with different capacities on the Cu foil show that the Li metal deposited in DME-LiTFSI is loose and uneven, while the deposition of Li metal is dense and uniform in DME@FEC, which demonstrates better Li metal compatibility (Figure 7e). The Li||Cu half-cells are also assembled with DME-LiTFSI and DME@FEC for in situ Raman measurements to study the consumption of electrolyte components on the Cu foil surface during Li deposition. Figure 7b shows the characteristic peaks of two electrolytes in the Raman spectra. In the DME-LiTFSI electrolyte, the intensity of C−O−C is fixed, and the relative strength of the $TFSI^-$ anions gradually decreased with the deposition, indicating that the $TFSI^-$ anions are continuously consumed (Figure 7c). In DME@FEC, the characteristic peaks of FEC weakened slightly in the early stage, while the relative contents of the remaining characteristic peaks remain stable, indicating that FEC preferentially forms a stable SEI on the LMA surface, effectively slowing down the interfacial reaction consumption of $TFSI^-$ and solvent (Figure 7d). The symmetrical cell results indicate that the Li||DME@FEC||Li cells exhibit a lower polarization voltage (Figure 7f), longer cycle stability, smaller R_t value (Figures 7g and S26), and higher CCD than Li||DME@LiTFSI||Li cells (Figure 7h). This is because the SEI modified by FEC could homogenize the Li deposition behavior, slow down the volume expansion in the LMA, and effectively alleviate the continuous rise of polarization voltage during long cycling.

To gain deeper insight into the reaction process and mechanism of FEC in the liquid system, we systematically

Downloaded from pubs.acs.org/jacsat/article-pdf/doi/10.1021/jacs.6c16437/69193451/jacs.6c16437.pdf by XIAMEN UNIV. Jinbao Zhao on 15 November 2026

https://doi.org/10.1021/jacs.6c16437
J. Am. Chem. Soc. XXXX, XXX, XXX−XXX

characterize the SEI evolution on the LMA after resting and electrochemical cycling for various periods in the two electrolytes at room temperature, following the same protocol as used for the solid-state system. We further characterized the SEI evolution in the liquid electrolytes by XPS. In the FEC-free DME-LiTFSI electrolyte, the content of organic fluoride ($-CF_x$) remains high and Li_2O content increases continuously during resting (Figure S27), indicative of persistent $TFSI^-$ decomposition and accumulation of byproducts at the anode, which drives continuous and drastic compositional changes in the SEI. In contrast, for the DME@FEC electrolyte, the LiF content increases steadily with resting time, while the other components remain relatively stable (Figure S28), a trend fully consistent with that observed in the PEO@Dry-10%FEC. These results confirm that FEC preferentially reacts with Li metal to establish a LiF-rich SEI framework, which effectively suppresses the continuous decomposition of $TFSI^-$ and solvent at the LMA interface, reduces harmful byproduct accumulation, and mitigates the loss of active species, thereby benefiting long-term cycling stability. Upon cycling, the SEI in DME-LiTFSI remains dominated by organic components, with $-CF_x$ content persistently high (Figure 7i). By contrast, in the DME@FEC electrolyte, the LiF content increases steadily with cycling, while the relative contents of other components, including $-CF_x$ remain dynamically stable (Figure 7j). These observations indicate that FEC constructs a rigid, inorganic-rich SEI on the LMA, which prevents continuous consumption of $TFSI^-$ and solvent, and sustains long-term interfacial stability. Quantitative elemental analysis further supports this picture. In the DME@FEC system, the F content increases progressively with cycling, while C and O contents show only minor fluctuations (Figure 7k), confirming that the SEI is built upon a stable inorganic backbone. In contrast, the DME-LiTFSI system exhibits a gradual decline in F content and a continuous rise in C and O contents (Figure 7l), indicating that the SEI is predominantly organic in nature.

Comparison of the SEI evolution in the PEO@Dry-10%FEC and DME@FEC systems reveals a higher LiF content and a lower abundance of $-CF_x$ species in the solvent-free PEO@Dry. As LiF originates from FEC reduction, whereas $-CF_x$ is derived from $TFSI^-$ decomposition, these results indicate that FEC dominates the interfacial reduction chemistry in the solid-state system, effectively suppressing Li salt decomposition. This behavior arises from the restricted of PEO@Dry, where free FEC molecules preferentially reach and react at the Li surface. In contrast, the high mobility of solvent molecules and other electrolyte species in the liquid electrolyte promotes competing interfacial reactions and increases $TFSI^-$ decomposition. Nevertheless, FEC follows the same fundamental mechanism in both systems, forming a LiF-rich SEI that facilitates Li^+ transport and stabilizes the Li metal interface. The performance differences therefore originate from transport kinetics rather than the intrinsic film-forming chemistry of FEC. The performance differences between the solid and liquid systems arise primarily from variations in the physical state, mobility, and reaction kinetics of FEC rather than from any fundamental change in its film-forming mechanism.

The results above demonstrate that FEC stabilizes the electrode/electrolyte interface by constructing a LiF-rich SEI on the LMA through chemical and electrochemical reactions, in both solid and liquid electrolytes. In the solid polymer electrolyte (SPE) system, free FEC reacts preferentially with Li metal, resulting in an SEI inner layer composed almost entirely of LiF. In the liquid electrolyte, a small amount of solvent inevitably participates in interfacial reactions, yielding an SEI inner layer that is predominantly LiF with a minor organic component. Consequently, the LiF enrichment is more pronounced in the SPE system, leading to more efficient Li^+ interfacial transport. To directly validate the beneficial role of the LiF-rich SEI, we preformed such an interfacial layer on the Li metal anode. Li||PEO@Dry-10%FEC||Li symmetric cells are assembled, allowed to stand for 24 h, and then cycled for 10 cycles at 60 °C (0.1 mA cm^{-2}, 0.1 mA h cm^{-2}) to ensure full formation of a LiF-rich SEI on the anode. After this pretreatment, the symmetric cells are disassembled, and the Li metal with a surface-enriched LiF layer (designated Li@LiF) is retrieved (Figure 7m). Using DME-LiTFSI as the electrolyte, the Li@LiF anode is paired with a $LiFePO_4$ (LFP) cathode to assemble half-cells. The LFP||DME-LiTFSI||Anode (Li@LiF) cells deliver stable electrochemical performance over 500 cycles at a high rate of 2.0 C (Figure 7n) and exhibit excellent rate capability, maintaining stable high capacities even at elevated current densities (Figure 7o). These results further confirm the film-forming function of FEC and the critical role of LiF in promoting Li^+ transport across the SEI.

CONCLUSIONS

In summary, we have employed a solvent-free PEO@Dry electrolyte as a model platform to isolate and investigate the intrinsic interfacial reaction mechanism of FEC on the LMA, eliminating the interference of other solvent components. Our results reveal that FEC undergoes both chemical and electrochemical reactions with Li metal, with the electrochemical pathway proceeding at a significantly faster rate. The SEI evolution demonstrates that FEC preferentially reacts with Li metal to form a rigid LiF-rich inorganic framework, upon which a stable organic−inorganic composite SEI is subsequently built. This SEI effectively stabilizes the anode interface and mitigates the degradation of the Li metal. As a result, the Li||PEO@Dry-10%FEC||Li symmetric cell delivers a stable cycling life of 1800 h at 0.1 mA cm^{-2}, and the Li||LFP half-cell retains 88.7% of its initial capacity after 200 cycles at 0.2 C, whereas the FEC-free PEO@Dry cell shows significant capacity decay after only 60 cycles.

Beyond the solid-state system, we also constructed a liquid-phase analogue (DME-LiTFSI) with a similar chemical composition but fundamentally different transport environments to verify the generality of the FEC mechanism. The results confirm that FEC functions consistently in both solid and liquid electrolytes, demonstrating that its beneficial effects on the LMA can reduce interfacial heterogeneity, mitigate local current concentration, and suppress the decomposition of Li salts and solvents through the formation of a mechanically robust and ionically conductive SEI, and are not limited by the physical state of the electrolyte.

It is worth emphasizing that the role of FEC in SEI formation differs fundamentally depending on its involvement in Li^+ solvation. In our solvent-free PEO-based system, FEC remains as a free molecule without coordinating to Li^+, allowing it to chemically react with Li metal during the resting stage and preform a LiF-rich inorganic framework prior to any electrochemical process. Subsequent electrochemical reduction further reinforces this framework. In contrast, in liquid electrolytes, FEC partially enters the Li^+ solvation sheath, and its reductive decomposition is accompanied by competitive reactions with other electrolyte species such as $TFSI^-$,

Downloaded from pubs.acs.org/jacsat/article-pdf/doi/10.1021/jacs.6c16437/6919345/1/jacs.6c16437.pdf by XIAMEN UNIV, Jinbao Zhao on 15 November 2026

https://doi.org/10.1021/jacs.6c16437
J. Am. Chem. Soc. XXXX, XXX, XXX−XXX

resulting in a more mixed organic/inorganic SEI composition. This comparison confirms that the solvation state of FEC critically dictates its interfacial reaction pathway and SEI formation mechanism.

Methodologically, this work establishes a new paradigm for studying additive interfacial chemistry: using a solvent-free solid electrolyte as a chemically well-defined model system to deconvolute the intrinsic reactions of a single component, followed by validation in a liquid analogue to confirm its generality. This approach not only resolves the long-standing difficulty of disentangling additive contributions in multi-component liquid electrolytes but also provides a transferable framework for investigating the interfacial mechanisms of other electrolyte additives on reactive metal anodes.

■ ASSOCIATED CONTENT

Supporting Information

The Supporting Information is available free of charge at https://pubs.acs.org/doi/10.1021/jacs.6c16437.

The data for experiments and test methods, Raman spectra, FTIR spectra, ionic conductivity curves, CV curves, transference number curves, Tafel curves, EIS spectra, optical pictures, SEM images, cycling curves, and XPS spectra (PDF)

■ AUTHOR INFORMATION

Corresponding Authors

Peng Zhang − *College of Energy, Xiamen University, Xiamen 361102, P. R. China*; Email: pengzhang@xmu.edu.cn

Jinbao Zhao − *College of Chemistry and Chemical Engineering, Xiamen University, Xiamen 361005, P. R. China; State−Province Joint Engineering Laboratory of Power Source Technology for New Energy Vehicle, State Key Laboratory of Physical Chemistry of Solid Surfaces, Engineering Research Center of Electrochemical Technology, Ministry of Education, Collaborative Innovation Center of Chemistry for Energy Materials, Xiamen University, Xiamen 361005, P. R. China; Innovation Laboratory for Sciences and Technologies of Energy Materials of Fujian Province (IKKEM), Xiamen 361005, P. R.China;* orcid.org/0000-0002-2753-7508; Email: jbzhao@xmu.edu.cn

Authors

Nanbiao Pei − *College of Chemistry and Chemical Engineering, Xiamen University, Xiamen 361005, P. R. China*

Yuan Tian − *College of Chemistry and Chemical Engineering, Xiamen University, Xiamen 361005, P. R. China*

Xueying Yang − *College of Energy, Xiamen University, Xiamen 361102, P. R. China*

Qijie Gao − *College of Chemistry and Chemical Engineering, Xiamen University, Xiamen 361005, P. R. China*

Yaqi Zhang − *College of Chemistry and Chemical Engineering, Xiamen University, Xiamen 361005, P. R. China*

Zhibin Lin − *College of Energy, Xiamen University, Xiamen 361102, P. R. China*

Yu Qiao − *College of Chemistry and Chemical Engineering, Xiamen University, Xiamen 361005, P. R. China; Innovation Laboratory for Sciences and Technologies of Energy Materials of Fujian Province (IKKEM), Xiamen 361005, P. R.China;* orcid.org/0000-0002-2191-3875

Complete contact information is available at: https://pubs.acs.org/10.1021/jacs.6c16437

Notes

The authors declare no competing financial interest.

■ ACKNOWLEDGMENTS

The authors gratefully acknowledge financial support from the National Key Research and Development Program of China (Grant No. 2021YFB2400300), the National Natural Science Foundation of China (Grant Nos. 21875195, 21875198, 22005257, and 22021001), the Fundamental Research Funds for the Central Universities (20720190040). This project has been approved by the Key Research and Development Program of the Yunnan Provincial Department of Science and Technology (Grant No. 202403AA080018). And the authors also would like to express gratitude for the support of the Tan Kah Kee Innovation Laboratory.

■ REFERENCES

(1) Goodenough, J. B. Electrochemical energy storage in a sustainable modern society. *Energy Environ. Sci.* **2014**, *7* (1), 14−18.

(2) Deng, D. Li-ion batteries: basics, progress, and challenges. *Energy Sci. Eng.* **2015**, *3* (5), 385−418.

(3) Etacheri, V.; Marom, R.; Elazari, R.; Salitra, G.; Aurbach, D. Challenges in the development of advanced Li-ion batteries: a review. *Energy Environ. Sci.* **2011**, *4* (9), 3243−3262.

(4) Mauger, A.; Julien, C. M. Critical review on lithium-ion batteries: are they safe? Sustainable? *Ionics* **2017**, *23* (8), 1933−1947.

(5) Zhu, Z.; Men, Y.; Zhang, W.; Yang, W.; Wang, F.; Zhang, Y.; Zhang, Y.; Zeng, X.; Xiao, J.; Tang, C.; Li, X.; Zhang, Y.-J. Versatile carbon-based materials from biomass for advanced electrochemical energy storage systems. *eScience* **2024**, *4* (5), 100249.

(6) Muldoon, J.; Bucur, C. B.; Gregory, T. Quest for Nonaqueous Multivalent Secondary Batteries: Magnesium and Beyond. *Chem. Rev.* **2014**, *114* (23), 11683−11720.

(7) Cheng, X. B.; Zhang, R.; Zhao, C. Z.; Wei, F.; Zhang, J. G.; Zhang, Q. A Review of Solid Electrolyte Interphases on Lithium Metal Anode. *Adv. Sci.* **2016**, *3* (3), 1500213.

(8) Ding, J. F.; Xu, R.; Ma, X. X.; Xiao, Y.; Yao, Y. X.; Yan, C.; Huang, J. Q. Quantification of the Dynamic Interface Evolution in High-Efficiency Working Li-Metal Batteries. *Angew. Chem., Int. Ed.* **2022**, *61* (13), No. e202115602.

(9) Lu, Y.; Tu, Z.; Archer, L. A. Stable lithium electrodeposition in liquid and nanoporous solid electrolytes. *Nat. Mater.* **2014**, *13* (10), 961−969.

(10) Chen, X. R.; Zhao, B. C.; Yan, C.; Zhang, Q. Review on Li Deposition in Working Batteries: From Nucleation to Early Growth. *Adv. Mater.* **2021**, *33* (8), 2004128.

(11) Fang, R.; Zhao, S.; Sun, Z.; Wang, D. W.; Cheng, H. M.; Li, F. More Reliable Lithium-Sulfur Batteries: Status, Solutions and Prospects. *Adv. Mater.* **2017**, *29* (48), 1606823.

(12) Fang, C.; Li, J.; Zhang, M.; Zhang, Y.; Yang, F.; Lee, J.Z.; Lee, M.H.; Alvarado, J.; Schroeder, M.A.; Yang, Y.; Lu, B Y.-S.Quantifying inactive lithium in lithium metal batteries. *Nature* **2019**, *572* (7770), 511−515.

(13) Ma, T.; Ni, Y.; Wang, Q.; Xiao, J.; Huang, Z.; Tao, Z.; Chen, J. Lithium dendrites inhibition by regulating electrodeposition kinetics. *Energy Storage Mater.* **2022**, *52*, 69−75.

(14) Sanchez, A. J.; Dasgupta, N. P. Lithium Metal Anodes: Advancing our Mechanistic Understanding of Cycling Phenomena in Liquid and Solid Electrolytes. *J. Am. Chem. Soc.* **2024**, *146* (7), 4282−4300.

(15) Yan, K.; Lu, Z.; Lee, H.-W.; Xiong, F.; Hsu, P.-C.; Li, Y.; Zhao, J.; Chu, S.; Cui, Y. Selective deposition and stable encapsulation of lithium through heterogeneous seeded growth. *Nat. Energy* **2016**, *1* (3), 16010.

Downloaded from pubs.acs.org/jacsat/article-pdf/doi/10.1021/jacs.6c16437/6919345l/jacs.6c16437.pdf by XIAMEN UNIV., Jinbao Zhao on 15 November 2026

(16) Pei, A.; Zheng, G.; Shi, F.; Li, Y.; Cui, Y. Nanoscale Nucleation and Growth of Electrodeposited Lithium Metal. *Nano Lett.* **2017**, *17* (2), 1132−1139.
(17) Liu, J.; Sun, B.; Zhao, L.; Liu, K.; Demicoli, M.; Song, J. Overcoming the Electrolyte-Derived Interphase Through Sequential Reactions for Stable Lithium Metal Anode. *J. Am. Chem. Soc.* **2025**, *147* (25), 21885−21895.
(18) Wang, Y. N.; Liu, Y.; Zhang, X. Q.; Sun, S. Y.; Li, Y.; Li, J. L.; Zhang, Q. K.; Zheng, Z.; Feng, W. J.; Li, B. Q.; Cheng, T.; Wen, R.; Huang, J.-Q. In Situ Polymerized Polysiloxane Enables Cohesive Solid-Electrolyte Interphase for Practical Lithium-Metal Batteries. *Adv. Mater.* **2025**, *38* (10), No. e19565.
(19) Zhang, Q.-K.; Li, Y.; Yu, P.-P.; Zhang, X.-Q.; Wang, Y.-N.; Zhao, Y.-X.; Sun, S.-Y.; Li, J.-L.; Ding, X.-Q.; Zheng, Z.; Feng, W.-J.; Yao, N.; Li, B.-Q.; Peng, H.-J.; Cheng, X.-B.; Wen, R.; Cheng, T.; Zhang, Q.; Huang, J. Q. Accelerated Defluorination Kinetics for an Ultrathin Solid−Electrolyte Interphase in Durable Lithium Metal Batteries. *J. Am. Chem. Soc.* **2026**, *148* (7), 6915−6925.
(20) Xu, K. Electrolytes and interphases in Li-ion batteries and beyond. *Chem. Rev.* **2014**, *114* (23), 11503−11618.
(21) Xu, K. Interfaces and interphases in batteries. *J. Power Sources* **2023**, *559*, 232652.
(22) Heine, J.; Hilbig, P.; Qi, X.; Niehoff, P.; Winter, M.; Bieker, P. Fluoroethylene Carbonate as Electrolyte Additive in Tetraethylene Glycol Dimethyl Ether Based Electrolytes for Application in Lithium Ion and Lithium Metal Batteries. *J. Electrochem. Soc.* **2015**, *162* (6), A1094−A1101.
(23) Dachraoui, W.; Kühnel, R.-S.; Kummer, N.; Battaglia, C.; Erni, R. Enhanced Solid Electrolyte Interphase Layer in Li-Ion Batteries with Fluoroethylene Carbonate Additives Evidenced by Liquid-Phase Transmission Electron Microscopy. *ACS Nano.* **2025**, *19* (20), 19213−19224.
(24) Ota, H.; Shima, K.; Ue, M.; Yamaki, J.-I. Effect of vinylene carbonate as additive to electrolyte for lithium metal anode. *Electrochim. Acta.* **2004**, *49* (4), 565−572.
(25) Ota, H.; Sakata, Y.; Otake, Y.; Shima, K.; Ue, M.; Yamaki, J.-I. Structural and Functional Analysis of Surface Film on Li Anode in Vinylene Carbonate-Containing Electrolyte. *J. Electrochem. Soc.* **2004**, *151* (11), A1778−A1788.
(26) Yan, C.; Yao, Y. X.; Chen, X.; Cheng, X. B.; Zhang, X. Q.; Huang, J. Q.; Zhang, Q. Lithium Nitrate Solvation Chemistry in Carbonate Electrolyte Sustains High-Voltage Lithium Metal Batteries. *Angew. Chem., Int. Ed.* **2018**, *57* (43), 14055−14059.
(27) Aurbach, D.; Pollak, E.; Elazari, R.; Salitra, G.; Kelley, C. S.; Affinito, J. On the Surface Chemical Aspects of Very High Energy Density, Rechargeable Li−Sulfur Batteries. *J. Electrochem. Soc.* **2009**, *156* (8), A694.
(28) Zhang, C.; Gu, S.; Zhang, D.; Ma, J.; Zheng, H.; Zheng, M.; Lv, R.; Yu, K.; Wu, J.; Wang, X.; Yang, Q.-H.; Kang, F.-Y.; Lv, W. Nonflammable, localized high-concentration electrolyte towards a high-safety lithium metal battery. *Energy Storage Mater.* **2022**, *52*, 355−364.
(29) Jagger, B.; Pasta, M. Solid electrolyte interphases in lithium metal batteries. *Joule* **2023**, *7* (10), 2228−2244.
(30) Chen, Y.-P.; Chen, X.; Yao, N.; Zheng, Z.; Yu, L.; Gao, Y.-C.; Zhu, H.-B.; Wang, C.-L.; Yao, J.-H.; Zhang, Q. A molecular review on weakly solvating electrolytes for lithium batteries. *Mater. Today* **2025**, *85*, 304−318.
(31) Heiskanen, S. K.; Kim, J.; Lucht, B. L. Generation and Evolution of the Solid Electrolyte Interphase of Lithium-Ion Batteries. *Joule* **2019**, *3* (10), 2322−2333.
(32) Wang, Q.; Zhao, C.; Wang, S.; Wang, J.; Wu, F.; Ombrini, P.; Ganapathy, S.; Eustace, S.; Bai, X.; Li, B.; Armand, M.; Aurbach, D.; Wagemaker, M. Interphase Design for Lithium-Metal Anodes. *J. Am. Chem. Soc.* **2025**, *147* (11), 9365−9377.
(33) Liao, D. W.; Zeng, D.; Mishra, G. K.; Lee, S. Y.; Melemed, A. M.; Penley, D.; Iwamura, R.; Kawakami, H.; Aihara, Y.; Aotani, K.; Dasgupta, N. Solid−Gas Interphase Formation in Anode-Free Solid-State Batteries. *J. Am. Chem. Soc.* **2025**, *147* (52), 48013−48027.
(34) Pang, L.; Li, H.; Feng, X.; Zhao, Z.; Ouyang, C.; Peng, Z. Operando Pulse Electrochemical Mass Spectrometry for Non-destructive and Long-Term Gas Analysis in Practical Lithium-Ion Pouch Batteries. *ACS Energy Lett.* **2024**, *9* (7), 3587−3594.
(35) Sharon, D.; Bennington, P.; Webb, M. A.; Deng, C.; de Pablo, J. J.; Patel, S. N.; Nealey, P. F. Molecular Level Differences in Ionic Solvation and Transport Behavior in Ethylene Oxide-Based Homopolymer and Block Copolymer Electrolytes. *J. Am. Chem. Soc.* **2021**, *143* (8), 3180−3190.
(36) Hakem, I. F.; Lal, J.; Bockstaller, M. R. Mixed solvent effect on lithium-coordination to poly(ethylene oxide). *J. Polym. Sci., Part B: Polym. Phys.* **2006**, *44* (24), 3642−3650.
(37) Pan, J.; Zhao, P.; Wang, N.; Huang, F.; Dou, S. Research progress in stable interfacial constructions between composite polymer electrolytes and electrodes. *Energy Environ. Sci.* **2022**, *15* (7), 2753−2775.
(38) Waugh, J. B.; Redko, M.; Jin, X.; Muldoon, G.; Kovrigin, E. L.; Gallant, B. M.; Li, Y.; Liu, G.; Muldoon, J. Overcoming misconceptions in lithium metal polymer electrolyte batteries. *Energy Environ. Sci.* **2025**, *18* (21), 9312−9323.
(39) Shao, Y.; Gudla, H.; Brandell, D.; Zhang, C. Transference Number in Polymer Electrolytes: Mind the Reference-Frame Gap. *J. Am. Chem. Soc.* **2022**, *144* (17), 7583−7587.
(40) Zhu, J.; He, S.; Tian, H.; Hu, Y.; Xin, C.; Xie, X.; Zhang, L.; Gao, J.; Hao, S. M.; Zhou, W.; Zhang, L.-Q. The Influences of DMF Content in Composite Polymer Electrolytes on Li^+-Conductivity and Interfacial Stability with Li-Metal. *Adv. Funct. Mater.* **2023**, *33* (25), 2301165.
(41) Foran, G.; Mankovsky, D.; Verdier, N.; Lepage, D.; Prébé, A.; Aymé-Perrot, D.; Dollé, M. The Impact of Absorbed Solvent on the Performance of Solid Polymer Electrolytes for Use in Solid-State Lithium Batteries. *iScience* **2020**, *23* (10), 101597.
(42) Lu, Y.; Zhao, C.-Z.; Yuan, H.; Cheng, X.-B.; Huang, J.-Q.; Zhang, Q. Critical Current Density in Solid-State Lithium Metal Batteries: Mechanism, Influences, and Strategies. *Adv. Funct. Mater.* **2021**, *31* (18), 2009925.
(43) Schiele, A.; Breitung, B.; Hatsukade, T.; Berkes, B. Z. B.; Hartmann, P.; Janek, J. R.; Brezesinski, T. The Critical Role of Fluoroethylene Carbonate in the Gassing of Silicon Anodes for Lithium-Ion Batteries. *ACS Energy Lett.* **2017**, *2* (10), 2228−2233.
(44) Hobold, G. M.; Khurram, A.; Gallant, B. M. Operando Gas Monitoring of Solid Electrolyte Interphase Reactions on Lithium. *Chem. Mater.* **2020**, *32* (6), 2341−2352.
(45) Kim, K.; Park, I.; Ha, S.-Y.; Kim, Y.; Woo, M.-H.; Jeong, M.-H.; Shin, W. C.; Ue, M.; Hong, S. Y.; Choi, N.-S. Understanding the thermal instability of fluoroethylene carbonate in $LiPF_6$-based electrolytes for lithium ion batteries. *Electrochim. Acta.* **2017**, *225*, 358−368.

Downloaded from pubs.acs.org/jacsat/article-pdf/doi/10.1021/jacs.6c16437/6919345l/jacs.6c16437.pdf by XIAMEN UNIV. Jinbao Zhao on 15 November 2026

https://doi.org/10.1021/jacs.6c16437
J. Am. Chem. Soc. XXXX, XXX, XXX−XXX